# Functional Characterization of Peanut Serine/Threonine/Tyrosine Protein Kinase: Molecular Docking and Inhibition Kinetics with Tyrosine Kinase Inhibitors†

Parvathi Rudrabhatla and Ram Rajasekharan*

*Department of Biochemistry, Indian Institute of Science, Bangalore 560012, India*

*Received February 10, 2004; Revised Manuscript Received July 26, 2004*

ABSTRACT: Serine/threonine/tyrosine (STY) protein kinase from peanut is developmentally regulated and is induced by abiotic stresses. In addition, STY protein kinase activity is regulated by tyrosine phosphorylation. Kinetic mechanism of plant dual specificity protein kinases is not studied so far. Recombinant STY protein kinase occurs as a monomer in solution as shown by gel filtration chromatography. The relative phosphorylation rate of kinase against increasing enzyme concentrations follows a first-order kinetics indicating an intramolecular phosphorylation mechanism. Moreover, the active recombinant STY protein kinase could not transphosphorylate a kinase-deficient mutant of STY protein kinase. Molecular docking studies revealed that the tyrosine kinase inhibitors bind the protein kinase at the same region as ATP. STY protein kinase activity was inhibited by the tyrosine kinase inhibitors, and the inhibitor potency series against the recombinant STY protein kinase was tyrphostin > genistein > staurosporine. The inhibition constant ($K_i$), and the $IC_{50}$ value of STY protein kinase for tyrosine kinase inhibitors with ATP and histone are discussed. All the inhibitors competed with ATP. Genistein was an uncompetitive inhibitor with histone, whereas staurosporine and tyrphostin were linear mixed type noncompetitive inhibitors with histone. Molecular docking and kinetic analysis revealed that Y148F mutant of the "ATP-binding loop" and Y297F mutant of the "activation loop" showed a dramatic increase in $K_i$ values for genistein and tyrphostin with respect to wild-type STY protein kinase. Data presented here provide the direct evidence on the mechanism of inhibition of plant protein kinases by tyrosine kinase inhibitors. This study also suggests that tyrosine kinase inhibitors may be useful in unraveling the plant tyrosine phosphorylation signaling cascades.

Tyrosine phosphorylation plays an important role in the regulation of many cellular processes. Tyrosine kinases are enzymes within the cell that function to transfer a phosphate group to the amino acid tyrosine. This process of phosphorylation serves two primary roles: as a molecular on−off switch and as a connector that binds proteins to one another. In these roles, tyrosine kinases can trigger a cascade of cellular events when phosphorylation stimulates additional enzymes, or when it prompts proteins to change their location. Tyrosine phosphorylation is therefore an early event in a complex signaling system that transfers information from outside the cell into the nucleus. On the basis of this incoming information, cells respond in many ways, the most basic of which is to live or die (*1*). No classical tyrosine kinase has hitherto been cloned from plants. We have recently reported that the stress responsive peanut dual specificity kinase is regulated by tyrosine phosphorylation (*2*, *3*).

Specific inhibitors of protein tyrosine kinases (PTKs)[1] provide a useful means to examine the role of tyrosine phosphorylation in a variety of cellular events. Enhanced PTK activity due to activating mutations or overexpression has been implicated in many human cancers (*4*). Thus, selective inhibitors of PTKs have considerable therapeutic value (*5*). Although a number of compounds have been identified as effective inhibitors of specific PTKs, the precise molecular mechanism by which these agents inhibit PTK activity has not been elucidated.

Tyrosine kinase inhibitors act by competing with ATP for binding to the kinase. This is possible because of structural similarities between ATP and the inhibitors. Kinases use ATP as the source of phosphate, but if an inhibitor binds to the enzyme instead of ATP, then the kinase cannot phosphorylate proteins and therefore the signaling halts. There are several different kinds of inhibitors that function in this manner, but the most commonly used are genistein, staurosporine, and tyrphostins. Genistein, 4′,5,7-trihydroxyisoflavone, is a potent specific inhibitor of tyrosine-dependent protein kinases, including the EGF (epidermal growth factor) receptor kinase and pp60 v-src kinase, with almost no inhibition observed for serine- and threonine-dependent protein kinases (*6*). Tyrphostin 25, [(3,4,5-trihydroxyphenyl)-methylene]-propanedinitrile, is a potent inhibitor of EGF receptor protein

† This work was supported by grant from Department of Science and Technology, New Delhi, India. E-mail: lipid@biochem.iisc.ernet.in.

* To whom correspondence should be addressed. Telephone: +91−80−2932881, Fax: +91−80−23602627.

[1] Abbreviations: A-loop, activation loop; EGF, epidermal growth factor; $IC_{50}$, inhibitor concentration leading to 50% inhibition of an enzymatic reaction; $(His)_6$-STY, histidine fusion protein of STY protein kinase; MAP, mitogen activated protein; MBP, maltose-binding protein; Ni-NTA, nickel-nitrilotriacetic acid; PDB, protein data bank; PKA, cAMP-dependent protein kinase; PKC, protein kinase C; PTK, protein tyrosine kinase; STY, serine/threonine/tyrosine; Tyr, tyrosine; TEY, threonine-glutamate-tyrosine.

10.1021/bi0497042 CCC: $27.50 
Published on Web 08/31/2004

tyrosine kinase activity (*7*). Staurosporine has been shown to inhibit Ser/Thr as well as Tyr kinases (*8*, *9*). The effect of these inhibitors on animal tyrosine kinases has been well understood.

Staurosporine is shown to inhibit plant serine/threonine kinases (*10*); however, the effect of tyrphostin and genistein on plant protein kinases is not reported so far. As peanut STY protein kinase is regulated by tyrosine phosphorylation, we were interested to observe the mechanism of inhibition of this kinase by potent tyrosine kinase inhibitors. In this study, we show that recombinant STY protein kinase is inhibited by tyrphostin and genistein at nanomolar concentrations as observed for animal tyrosine kinases. STY protein kinase is phosphorylated at multiple sites, $Tyr^{148}$ of ATP binding motif, $Tyr^{213}$ of Thr-Glu-Tyr (TEY) domain, $Tyr^{297}$ of activation loop (A-loop), and $Tyr^{317}$ of C-terminal domain (*3*). Molecular docking and kinetic analysis of the tyrosine mutants of STY protein kinase revealed that $Tyr^{148}$, $Tyr^{213}$, and $Tyr^{297}$ are involved in binding to the inhibitors.

## EXPERIMENTAL PROCEDURES

*Materials.* Histone H1 (Type-IIIS) was purchased from Sigma Chemical Company, St. Louis. [$\gamma$-$^{32}$P]ATP (3000 Ci/mmol) was obtained from Perkin-Elmer Lifesciences, Boston, MA. Restriction endonucleases were from MBI Fermentas, St. Leon-Rot, Germany. Ni-NTA agarose was obtained from Qiagen, Hilden, Germany. Genistein (AG1478), tyrphostin (AG213), and staurosporine were obtained from CalBiochem, La Jolla, CA.

*Expression and Purification of Fusion Proteins.* The cDNA spanning for coding region of STY protein kinase was subcloned into the histidine-tagged fusion protein expression vector, pRSET C at *Bgl*II and *Kpn*1 restriction sites. The resultant construct was expressed in *Escherichia coli* BL21 (pLysS). The fusion protein was induced with 0.4 mM isopropyl-1-thio-$\beta$-D-galactopyranoside for 4 h. The recombinant protein was induced in large scale (500 mL) and purified by Ni-NTA agarose chromatography. Site-specific mutagenesis of K160R, Y148F, Y213F, Y297F, and Y317F of STY protein kinase were performed as described earlier (*3*). Expression and purification of histidine fusion proteins of mutant STY protein kinase were performed similar to wild type. The STY protein kinase-deficient form STY(K160R) was fused in frame to the C-terminus of the maltose-binding protein (MBP). MBP fusion was expressed in the *E. coli* strain PR745 (New England Biolabs) and affinity-purified by using amylose resin. Protein concentrations were determined by the Bradford method (*11*). Purified fractions containing the eluted protein were analyzed by 12% SDS−PAGE followed by Coomassie blue staining (*12*).

*Size Exclusion Chromatography.* Purified $His_6$-STY protein kinase (0.5 mg) was subjected to Superdex 200 HR 10/30 FPLC column. The column was equilibrated with buffer containing 20 mM Tris-HCl (pH 7.5), 150 mM NaCl. The column was eluted with 24 mL of the same buffer, and 0.4 mL fractions were collected. Protein concentration in the fractions was determined by absorbance at 280 nm. Molecular mass markers (all about 0.5 mg) used for calibrating column were as follows: thyroglobulin (669 kDa), ferritin (440 kDa), catalase (232 kDa), aldolase (158 kDa), BSA (67 kDa), ovalbumin (43 kDa), chymotrypsinogen A (25 kDa), and ribonuclease A (13.7 kDa). The elution volumes ($V_e$) of marker proteins and STY protein kinase were determined. The molecular mass of STY protein kinase was calculated from the plot of $V_e/V_o$ versus log of molecular mass.

*Homology Modeling.* Modeling of the structure of STY family protein kinase was performed based on the X-ray structures of the protein structures that produced the best E value when using BLAST against the protein in the protein data bank (PDB) database using the SwissPDB Viewer package (*13*; http://www.expasy.ch/swissmod/SWISS-MOD-EL.html). The molecular modeling method used was ProMod II (*13*). Three-dimensional models of STY protein kinase were predicted using the coordinates of chicken Src tyrosine kinase (PDB code 2PTK, determined at 2.35 Å; *14*), human Src (code 2SRC, 1.5 Å; *15*), mouse c-ABL kinase in complex with the inhibitor STI-571 (code 1IEPA, 2.1 Å; *16*), and mouse ABL tyrosine kinase with small molecule inhibitor (code 1FPU, 2.4 Å; *17*) protein kinase domains. The sequence of the kinase domain of STY protein kinase sequences were aligned with the sequence of the homologous tyrosine kinases using the advanced BLAST program (http://www.ncbi.nlm.nih.gov/BLAST/). Refinement of side chains and terminal chains was done using the Molecular Operation Environment (MOE) software package (Version 2001.01, Chemical Computing Group, Montreal, Canada). The generated model was then energy minimized in SYBYL (Tripos Associates, St. Louis, MO) using a three-stage protocol involving simplex, conjugate-gradient, and Powell minimization methods, by moving side chains alone, to relieve short contacts at the interprotomer interfaces. The quality of the three-dimensional model was evaluated using PROCHECK and Prosa II version 3.0 (*18*). Improvements in the model were obtained by an iterative sequence−structure alignment procedure, yielding the final sequence alignment between the STY protein kinase domain and homologous structures. The modeled structure was stable at room temperature during a 140 ps unconstrained full protein molecular dynamics simulations. Three-dimensional models were visualized by RasMol (*19*). Calculations were performed on Silicon Graphics IRIS 4D/25 workstations (http://www.sgi.com).

*Computational Docking and Molecular Dynamics Simulations.* Docking was performed in SGI FUEL machine (Single 700 MHz MIPS R16000, 512MB-4GB synchronous double-data RAM), using unbiased docking software AutoDock 3.0.3. This program allows for flexibility in the ligand structure but uses a rigid body protein approximation to speed up the calculation. AutoDock combines Monte Carlo-simulated annealing for conformational searching with a rapid, atomic resolution, grid-based method of energy evaluation utilizing the AMBER force field (*20*). The inhibitor coordinates were obtained from Cambridge structural database. Polar hydrogen atoms were added to the protein using the SYBYL modeling package (Tripos Associates, Inc.). Gasteiger charges were computed by SYBYL for each molecule individually. The header information (HEADER), Water (HOH), Ligands (HETATM), ions (IONS), records were removed from the receptor PDB coordinate file, and only the atom records were retained. Essential hydrogens were added; KOLLUA charges were computed, by BIOPOLYMER option in SYBYL. The modified files of inhibitors and STY protein kinase were saved as mol2 file.

Nonpolar hydrogens were removed from each inhibitor, and their partial atomic charges were united with the bonded carbon atoms. Docking computations were performed using the Lamarkian genetic algorithm with grid sizes 40 × 40 × 40 (grid spacing 0.375 Å), yielding 10 docked conformations per frame. Autotors3 was used to define the torsions for the inhibitors. The program deftors is used to define the torsion for small ligands. The number of individual population was set to 250 000, the maximum number of generation was set as 27 000, run was set to 10, and all other options were set as default. Typically, the 10 lowest energy coordinate sets were extracted for each inhibitor type and used for visualization in WebLab Viewer 5.0 (Molecular Simulation Inc.).

*In Vitro Kinase Assays and Inhibitor Studies.* Toward autophosphorylation assays, 400 ng of $(His)_6$-STY protein kinase fusion protein was preincubated with varying concentrations of inhibitors (0−50 nM) for 10 min. Then the incubation was continued with 0.1−500 $\mu$M ATP containing 2.5 $\mu$Ci of [$\gamma$-$^{32}$P]ATP (3000 Ci/mmol) in a total volume of 20 $\mu$L of kinase buffer (10 mM $MgC1_2$, 50 mM Tris-HCl) and stopped at 20 min by adding 10 $\mu$L of Laemmli loading buffer (3×). The reaction products were separated by 12% SDS−PAGE followed by autoradiography. The Coomassie blue-stained protein bands were recovered and then measured using a liquid scintillation counter.

The kinetic experiments with histone as the substrate with varying concentrations were performed with the prephosphorylated STY protein kinase that was prepared by preincubating 300 ng of $(His)_6$-STY protein kinase, 10 mM $MgC1_2$, and 50 $\mu$M ATP in 50 mM Tris-HCl (pH 7.5). The inhibitors (genistein, tyrphostin, and staurosporine), at the indicated concentration (0−1000 nM), were then added to the mixture, and the incubation was allowed to continue for 10 min. The reaction was initiated by adding 1 $\mu$Ci of [$\gamma$-$^{32}$P]-ATP (3000 Ci/mmol), and variable histone concentrations as indicated and reaction mixtures were immediately transferred to 30 °C for 20 min. The complete reaction mixture (30 L) was spotted onto a 2-cm square Whatman 3MM paper and immediately dropping the paper into a beaker of cold 10% trichloroacetic acid containing 0.01 M sodium pyrophosphate. Following four subsequent washes, 20 min each, the filter papers were washed extensively with pyrophosphate-containing 10% trichloroacetic acid at room temperature and extracted with alcohol, and the radioactivity was determined by liquid scintillation counting in 5 mL of toluene-based scintillation fluid using a Beckman model LS 5801 liquid scintillation counter (*21*). Assay of histone phosphorylation using the trichloroacetic acid precipitation method for determining the phosphate transfer performed either in the absence of STY protein kinase or in the absence of histone were used as controls. In addition, the histone phosphorylation performed at zero time was used as a control. However, the experiments were also performed by separating the histone phosphorylation reaction mix using 12% SDS−PAGE followed by autoradiography. The bands of histone were excised from the gel, and the radioactivity was counted in liquid scintillation counter and similar results were obtained.

Lineweaver−Burk double-reciprocal plots were generated by linear least-squares fits of the data. Data from inhibition experiments were fitted to either a linear competitive model

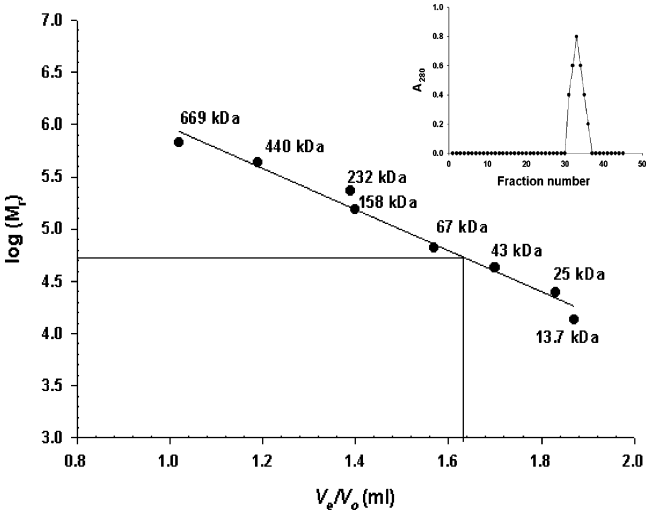


FIGURE 1: Determination of the molecular mass of STY protein kinase by gel filtration chromatography. Purified $(His)_6$-STY protein kinase (0.5 mg) was subjected to Superdex 200 HR 10/30 FPLC column. The standard curve, $V_e/V_o$ versus log molecular mass was derived from the elution profiles of standard molecular mass markers with $V_e$ corresponding to the peak elution volume of the protein. The flow rate was 0.3 mL/min, and the protein was monitored by the absorbance at 280 nm. STY protein kinase was eluted between BSA and ovalbumin. The peak position of STY protein kinase is indicated by a line. Inset shows the elution profile of STY protein kinase.

(eq 1) or a noncompetitive (or mixed) model (eq 2) or uncompetitive model (eq 3).

$$1/v = K_m/V_{max}(1 + I/K_i)1/S + 1/V_{max} \quad (1)$$

$$1/v = K_m/V_{max}(1 + [I]/K_{is})1/[S] + 1/V_{max}\,(1 + [I]/K_{ii}) \quad (2)$$

$$1/v = K_m/V_{max}(1)/[S] + 1/V_{max}\,(1 + [I]/K_i) \quad (3)$$

Accordingly, secondary plots were generated by replotting the slopes, the *x* intercepts, and the *y* intercepts of the lines as a function of inhibitor concentration. The values of $K_i$ were determined from the secondary plots (*22*). The values of $K_{ii}$ and $K_{is}$ can be determined from the secondary plots. $K_{is}$ is the apparent $K_i$ value that accounts for the change of the slope. $K_{ii}$ is the apparent $K_i$ value that accounts for the change of the *y* intercept.

## RESULTS

*Determination of Oligomeric Nature of $(His)_6$-STY Protein Kinase.* Gel filtration analysis was performed to determine the oligomeric nature of $(His)_6$-STY protein kinase in solution. STY protein kinase was chromatographed on a Superdex 200 column equilibrated with 20 mM Tris-HCl (pH 7.5), 150 mM NaCl. Reference proteins were used to generate a standard curve (Figure 1). STY protein kinase was eluted as a symmetric peak between the elution profile of bovine serum albumin and ovalbumin, with a molecular mass of 55 kDa, suggesting that the enzyme exists as monomer under native conditions.

*Autophosphorylation Mechanism of $(His)_6$-STY Protein Kinase.* Autophosphorylation of protein kinases might proceed by intra- or intermolecular mechanisms. To test whether the autophosphorylation of recombinant STY protein kinase

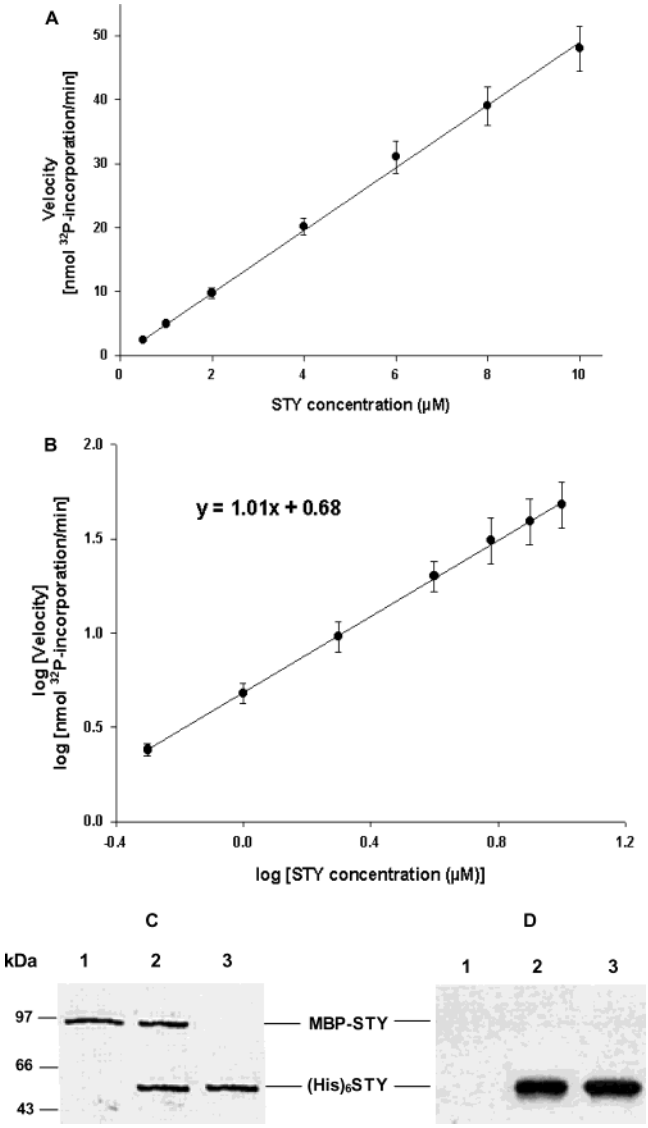


FIGURE 2: Intramolecular mechanism of phosphorylation of STY protein kinase. Autophosphorylation of recombinant STY protein kinase was tested at different enzyme concentrations in an in vitro kinase assay. The enzyme concentration varied from 0.5 to 10 $\mu$M. (A) Plot of phosphate incorporation rate versus STY protein kinase concentration in the assay. (B) van't Hoff plot of the algorithm of velocity versus the logarithm of STY protein concentration. Linear regression of the data in B estimated a slope of $1.01 \pm 0.08$ and a correlation coefficient of 0.99. In A and B, data are the mean $\pm$ SE ($n = 4$). (C) Intramolecular autophosphorylation assay of $(His)_6$-STY kinase and kinase-deficient MBP−STY kinase. Enzyme activities were tested in reactions containing the following combinations of fusion proteins: lane 1, the inactive MBP−STY(K160R) alone; lane 2, $(His)_6$-STY and the inactive MBP−STY(K160R); lane 3, $(His)_6$-STY kinase alone. Proteins were analyzed by SDS−PAGE and visualized by Coomassie staining. The autoradiography (D) shows the proteins phosphorylated in each assay. Sizes of the molecular mass markers are indicated on the left.

occurs via an intramolecular (first order with respect to enzyme concentration) mechanism, or an intermolecular (second order with respect to enzyme concentration) mechanism, autophosphorylation reaction was carried out in the presence of increasing concentrations of STY protein kinase. As shown in Figure 2A, the relative phosphorylation rate increases linearly with enzyme concentration, suggesting that the autophosphorylation follows first-order reaction kinetics. The van't Hoff analysis of autophosphorylation (logarithm of phosphorylation rate versus logarithm of enzyme concentration) illustrated a slope of $1.01 \pm 0.08$ and a correlation coefficient of 0.99 for linear regression (Figure 2B). To provide further evidence for intramolecular autophosphorylation by STY protein kinase, we tested if an active $(His)_6$-STY fusion protein can phosphorylate an inactive MBP−STY molecule in which the invariant lysine residue in kinase subdomain II was substituted by a arginine. As shown in Figure 2C,D, the $(His)_6$-STY fusion protein failed to phosphorylate the inactive mutant protein MBP−STY(K160R), strongly supporting the notion that STY autophosphorylation occurs through an intramolecular rather than intermolecular mechanism.

*Molecular Docking of STY Protein Kinase with Tyrosine Kinase Inhibitors.* A model for the molecular interaction of STY protein kinase with staurosporine and genistein is proposed. The use of molecular modeling and docking of small compounds into the target sites of molecular models derived directly from resolved crystal structures has proven valuable for studies on binding of inhibitors to protein kinases (*23*). Moreover, this approach has also been successful for molecular models based on homology to a protein of known structure (*24*). A three-dimensional model of STY protein kinase was predicted using the coordinates of chicken Src tyrosine kinase (PDB code 2PTK, determined at 2.35 Å; *13*), human Src (code 2SRC, 1.5 Å; *14*), mouse c-ABL kinase in complex with the inhibitor STI-571 (code 1IEPA, 2.1 Å; *15*), and mouse ABL tyrosine kinase with small molecule inhibitor (code 1FPU, 2.4 Å; *16*) protein kinase domains. The resulting model was energy minimized to convergence with SYBYL using a three-stage protocol involving simplex, conjugate-gradient, and Powell minimization methods. The *Z*-score of STY protein kinase three-dimensional model as determined by Prosa II implied that the model according to the quality assessment criteria developed by Sanchez and Sali (*25*) was very reliable (p(GOOD)/Q-SCORE) = 0.99). The PROCHECK evaluation of the model showed that 99% of the residues are in $\phi/\psi$ most favored/additionally allowed regions of the Ramachandran plot. In addition, the side chain parameters $x^{-1}$ and $x^{-2}$ determined by PROCHECK are better than protein X-ray crystal structures of model with 2.0 Å resolution. The modeled STY protein kinase domain has the expected protein kinase fold with the catalytic site in the center dividing the kinase domain into two lobes. It is composed of a smaller N-terminal lobe connected by a flexible hinge to a larger C-terminal lobe. The N-terminal lobe is rich in $\beta$-strands, whereas the C-terminal region is mostly helical. The catalytic site is defined by a loop that forms an interface at the cleft between the two lobes. It is in this catalytic region where the small molecule inhibitors can bind. The catalytic loop is the most conserved region. The nucleotide binding motif is contained in the small lobe (glycine-rich loop, $Lys^{160}$) (Figure 3A). The A-loop that spans between $Asp^{277}$ and $Glu^{303}$ packs between N-terminal and C-terminal lobes and sequesters $Tyr^{297}$. The modeled structure of STY protein kinase compared with the template tyrosine kinases showed strict similarity. This notion is further strengthened when the glycine loop, TEY domain, A-loop and C-terminal domain are examined in more detail (Figure 3A). The structure-based multiple sequence alignment of STY protein kinase with the tyrosine kinase

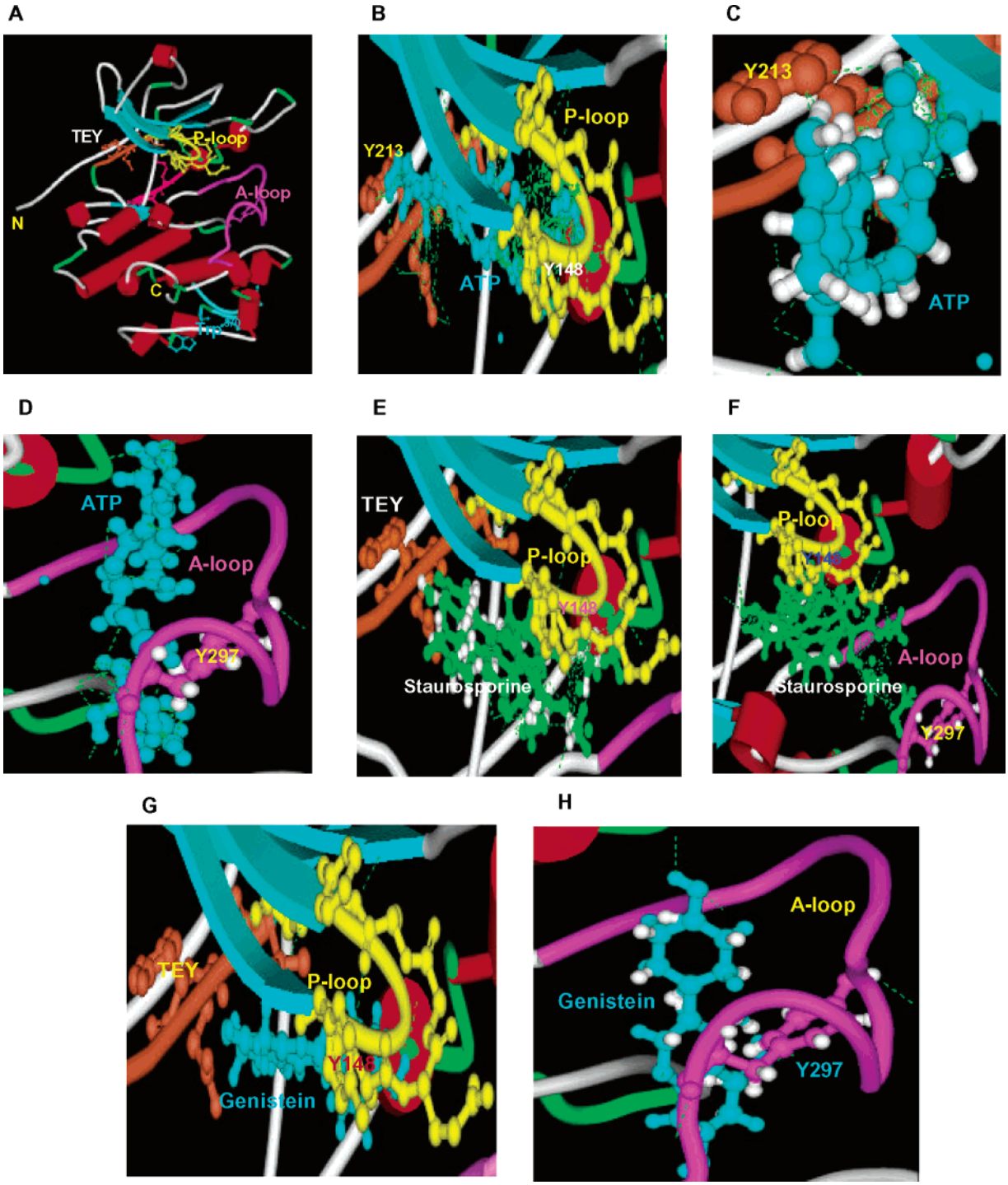


FIGURE 3: Molecular structure of the STY−ATP, STY−staurosporine, and STY−genistein complexes. Three-dimensional structure of the STY protein kinase catalytic domain from residues 138 to 382 was predicted with the Swiss-model program (*13*; http://www.expasy.ch/swissmod/SWISS-MODEL.html), using the coordinates for chicken Src tyrosine kinase (PDB code 2PTK, determined at 2.35 Å *14*), human Src (code 2SRC, 1.5 Å; *15*), mouse c-ABL kinase in complex with the inhibitor STI-571 (code 1IEPA, 2.1 Å; *16*), and mouse ABL tyrosine kinase with small molecule inhibitor (code 1FPU, 2.4 Å; *17*) protein kinase domains. (A) STY protein kinase nucleotide binding loop (yellow), TEY domain (orange), A-loop (pink), conserved $Trp^{370}$ (blue) are shown in modeled and minimized STY kinase molecule. α-Helices and *β*-strands are in red and blue, respectively. The complex structures of STY−ATP (B, C, and D), STY−staurosporine (E and F) and STY−genistein (G and H) were obtained from docking calculation using the AutoDock 3.0.3 program. Ball and stick representation of ATP, blue (B, C, and D), staurosporine, green (E and F) and genistein, blue (G and H), are positioned in the optimal docked orientation as determined from our computational results. Superposition of the $Tyr^{148}$ of the P-loop (yellow), $Tyr^{213}$ of TEY domain (orange), and $Tyr^{297}$ of A-loop (purple) of the STY protein kinase model and modeled minimized ATP, staurosporine, and genistein are depicted. The tyrosine residues, $Tyr^{148}$ (yellow), $Tyr^{213}$ (orange), and $Tyr^{297}$ (pink) are represented in ball-and-stick. Dashed green lines represent hydrogen bonds. These experiments were performed using the modified autogrid program and an additional "polar hydrogen" atom type. The complex structure above was generated in 7 out of 12 docking runs and had the best relative binding energy. The figures were prepared using WebLab ViewerLite.

templates used in this study revealed that the TEY motif, and the tyrosine kinase consensus $CW(X)_6RPXF$ are conserved (Figure 3A). These findings justified building a molecular model of STY protein kinase based on homology.

We applied the in silico macromolecular docking program, AutoDock 3.0.3, to dock the protein kinase domain with ATP and protein tyrosine kinase inhibitors. Application of AutoDock generated 10 docked structures per frame to give a total of 10 000 docked structures for each antagonist. The most frequent orientation produced by AutoDock has been shown for many protein−ligand complexes to agree well with the bound orientation observed in X-ray structures of the complexes. ATP binding sites in the crystal structures of basal state PTKs display various degrees of accessibility. STY protein kinase is phosphorylated at multiple sites such as $Tyr^{148}$ of ATP binding domain, $Tyr^{213}$ of TEY domain, $Tyr^{297}$ of A-loop, and $Tyr^{317}$ of C-terminal domain (*3*). Docking ATP into the STY protein kinase model yielded the expected good score (the more negative the value, the better the fit) with a fit close to the proposed ATP binding pocket (data not shown). ATP is sandwiched between $Tyr^{213}$ of TEY domain and $Tyr^{148}$ of nucleotide binding domain (Figure 3B). Docking studies also revealed a confirmation, where ATP is bound mainly to $Tyr^{213}$ of TEY domain of STY protein kinase molecule (Figure 3C). There is a single tyrosine in the A-loop of STY protein kinase. The interaction of $Tyr^{297}$ of the A-loop of STY protein kinase with ATP is shown in the Figure 3D. When we applied AutoDock to dock staurosporine with STY protein kinase, we observed that the staurosporine is sandwiched between $Tyr^{213}$ of TEY domain and $Tyr^{148}$ of ATP-binding loop (Figure 3E). The interaction of staurosporine with $Tyr^{148}$ of P-loop and $Tyr^{297}$ of A-loop is shown in Figure 3F. Docking studies revealed that genistein interacts with $Tyr^{148}$ of ATP binding motif (Figure 3G). The binding of $Tyr^{297}$ residue of A-loop of STY kinase with genistein is shown in Figure 3H. These results suggest that the tyrosine kinase inhibitors bind the protein kinase at the same region as ATP. In addition, docking studies revealed the interaction of protein kinase inhibitors with the tyrosine residues.

*Sensitivity of the Kinase Activity of the STY Kinase to Genistein, Tyrphostin, and Staurosporine.* As $(His)_6$-STY protein kinase predominantly autophosphorylated on tyrosine, we tested the enzyme with a panel of tyrosine kinase inhibitors. STY protein kinase was inhibited by the tyrphostin, genistein, and staurosporine in a dose-dependent manner, with the apparent $IC_{50}$ (the concentration of inhibitor which causes 50% inhibition) values of 50.07 ± 3.9, 64.45 ± 4.7, and 98.69 ± 7.8 nM, for ATP-dependent autophosphorylation, respectively (Figure 4A). Inhibitor potency series against STY protein kinase was tyrphostin > genistein > staurosporine (Figure 4A). The histone kinase activity of STY protein kinase was inhibited by tyrphostin, genistein, and staurosporine in a dose-dependent manner with the apparent $IC_{50}$ values of 429.71 ± 31.1, 571.23 ± 43.5, and 946.54 ± 71.2 nM, for histone phosphorylation, respectively (Figure 4B). These results support the finding that STY protein kinase phosphorylates on tyrosine.

*Staurosporine, Tyrphostin, and Genistein Are ATP-Competitive Inhibitors of STY Protein Kinase.* Double-reciprocal plot of $1/v$ versus 1/[ATP] at different concentrations of tyrphostin intersect on the ordinate, indicating that the inhibitor is competitive with ATP (Figure 5A). Replot of slope of the double reciprocal plot with inhibitor concentration was used to determine the $K_i$ of the inhibitor. Such a plot for STY protein kinase inhibition by tyrphostin is shown

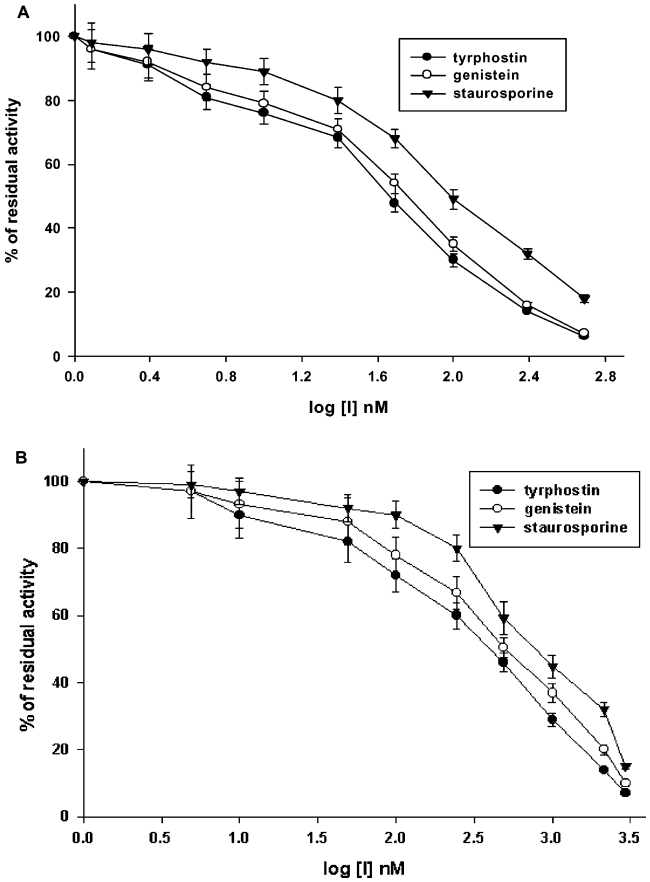


FIGURE 4: Inhibition of STY protein kinase activity by tyrosine kinase inhibitors. $(His)_6$-STY protein kinase was subjected to in vitro $^{32}P$-autophosphorylation in the presence of tyrosine kinase inhibitors. Tyrosine autophosphorylation of STY kinase was evaluated either in the absence (100%) or in the presence of increasing concentrations of indicated inhibitors. The concentration of ATP used in the assay was 50 $\mu$M, and the concentration of STY kinase used was 500 ng. (A) $IC_{50}$ plot of STY kinase in the presence of tyrphostin (●), genistein (○), and staurosporine (▼). (B) $IC_{50}$ plot of histone phosphorylation of STY kinase in the presence of tyrphostin (●), genistein (○), and staurosporine (▼). The concentration of histone used in the assay was 10 $\mu$M. The error bars represent the SD of three different experiments. The $IC_{50}$ curves were generated by SigmaPlot regression fitting using the equation: $y = 100\ (I_{max}x^n/(IC_{50}{}^n + x^n))$ ($x$ = [compound], $y$ = % activity, and $I_{max}$ is the maximum percentage of inhibition).

in Figure 5B. Similar plots were obtained for genistein and staurosporine inhibition of STY protein kinase (plot not shown). All the inhibitors competed with ATP. The $K_i$ values of tyrphostin, genistein, and staurosporine were determined to be 18.31 ± 1.5, 20.43 ± 1.3, and 69.12 ± 4.6 nM, respectively. The kinetic data corroborated well with docking analysis, suggesting a competitive inhibition of these inhibitors with ATP.

*Histone Phosphorylation Kinetics of STY Protein Kinase Inhibition by Tyrphostin, Genistein, and Staurosporine.* STY protein kinase activities were measured as a function of varying concentrations of histone at several different fixed concentrations of inhibitors (Figure 6). The Lineweaver−Burk plots of the data for STY protein kinase with tyrphostin and staurosporine indicated a linear mixed type noncompetitive inhibition pattern with the maximum velocity ($V_{max}$) reduced, and the apparent Michaelis constant ($K_m$) increased (Figure 6A,C). Replots of slope ($K_{is}$) and intercept ($K_{ii}$) of the double reciprocal plot with inhibitor concentration yielded

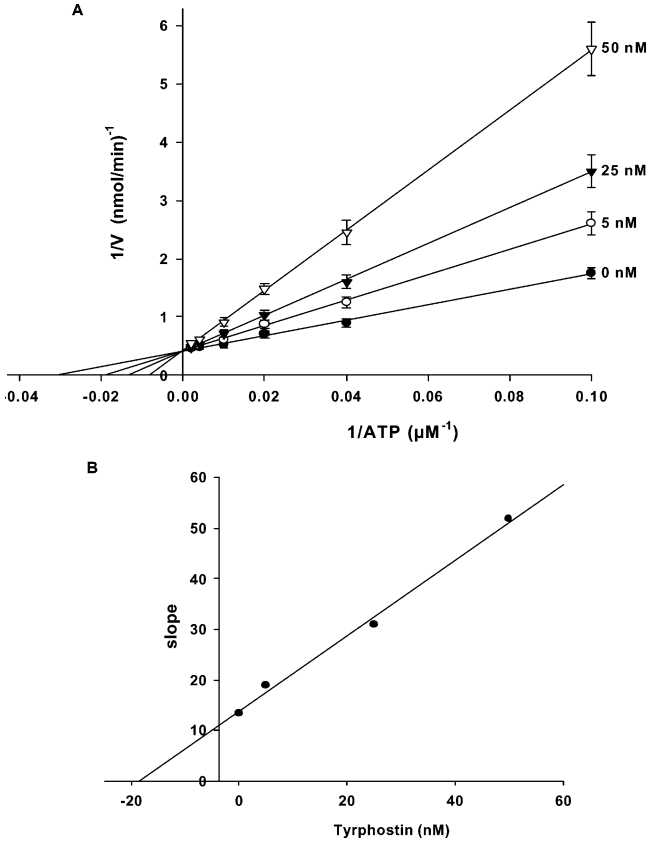


FIGURE 5: The kinetics of inhibition of STY protein kinase autophosphorylation by tyrphostin. (A) Double-reciprocal plot of $1/v$ versus 1/[ATP] was generated at fixed tyrphostin concentration. Reaction was performed at 30 °C for 15 min with 400 ng of $(His)_6$-STY protein kinase, 2.5 Ci of [$\gamma$-$^{32}$P]ATP, and varying concentrations of ATP as indicated. The error bars represent the SD of four different experiments. (B) The slopes of the plots in (A) were replotted versus [tyrphostin].

linear plots, suggesting a linear mixed-type inhibition. The replots of slope and *y* intercept of the double reciprocal plot with tyrphostin concentration yielded a $K_{is}$ value of 201.55 ± 19.1 nM and a $K_{ii}$ value of 539.17 ± 43.2 nM. The replot of slope and *y* intercept of the double reciprocal plot with staurosporine concentration yielded a $K_{is}$ value of 455.39 ± 34.7 nM and *a* $K_{ii}$ value of 997.12 ± 81.3 nM (plot not shown). Kinetic analysis of inhibitors by Dixon plots indicated a mixed inhibition pattern with the reduced maximum velocity ($V_{max}$), and the increased apparent Michaelis constant ($K_m$). The $K_i$ was also calculated from the Dixon secondary plot where the slopes at each substrate concentration of primary plots were plotted against the reciprocal substrate concentration (data not shown). The Lineweaver−Burk plots of the data for STY protein kinase with genistein yielded a series of linear and parallel straight lines to the left side of the ordinate, indicating an uncompetitive inhibition (Figure 6B). The replot of the *y* intercept of the double reciprocal plot with inhibitor concentration yielded a $K_i$ value of 426.33 ± 32.3 nM for genistein (Table 1).

*Kinetic Analysis of Tyrosine Mutants of STY Protein Kinase.* We have reported earlier that the tyrosine mutant proteins, Y148F of ATP binding motif, Y297F of A-loop, and Y317F of C-terminal kinase domain of STY protein kinase resulted in a drastic reduction in the protein kinase activity with respect to wild type (*3*). On the other hand, Y213F mutant protein of TEY domain is involved in

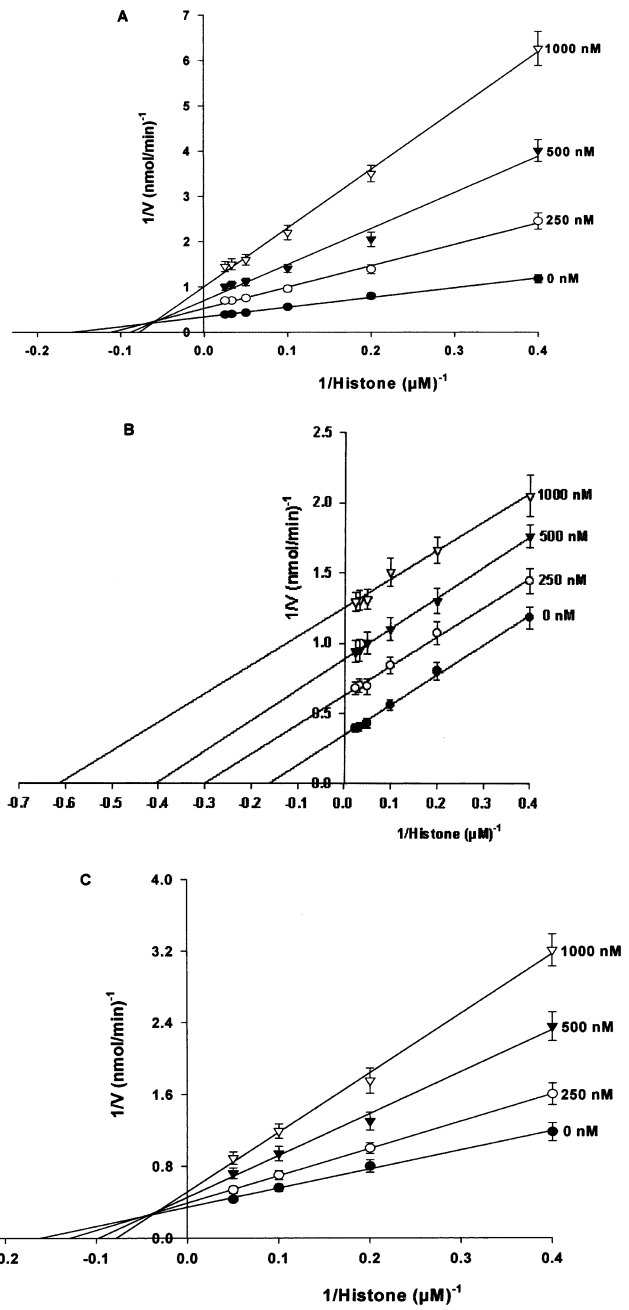


FIGURE 6: Kinetics of inhibition of histone phosphorylation by tyrphostin, genistein, and staurosporine. Double-reciprocal plots of $1/v$ versus 1/[histone] were generated at fixed concentrations of tyrosine kinase inhibitors. Reactions were performed at 30 °C for 15 min with 300 ng of $(His)_6$-STY protein kinase, 1 $\mu$Ci of [$\gamma$-$^{32}$P]-ATP, 50 $\mu$M of ATP, and varying concentrations of histone as indicated. Panels A−C represent the double-reciprocal plots of $1/v$ versus 1/[histone] at fixed concentrations of tyrphostin, genistein, and staurosporine, respectively. The error bars represent the SD of four different experiments.

autoinhibition (*3*). The inhibition constants of Y148F, Y213F, Y297F, and Y317F were determined for both ATP and histone to study the role of these residues in binding to the inhibitor.

Competitive inhibition was observed with ATP for all the mutant proteins with inhibitors. Y148F and Y297F mutant proteins resulted in dramatic increase in the $K_i$ value by 10-fold for genistein and tyrphostin toward ATP. The $K_i$ value of Y148F and Y297F mutant proteins is increased by 8- and 7-fold, respectively, for staurosporine toward ATP. The $K_i$

Table 1: Summary of Kinetic Parameters and Mode of Inhibition of STY Protein Kinase with Tyrosine Kinase Inhibitors

| | ATP [a] | | | histone[b] | | |
|---|---|---|---|---|---|---|
| inhibitor | $C_{50}$[c] (nM) | $K_i$ [d] (nM) | inhibition | $IC_{50}$ [c] (nM) | $K_i$ [d] (nM) | inhibition |
| tyrphostin | 50.07 ± 3.9 | 18.31 ± 1.5 | competitive | 429.71 ± 31.1 | 201.55 ± 19.1 | mixed[e] |
| genistein | 64.45 ± 4.7 | 20.43 ± 1.3 | competitive | 571.23 ± 43.5 | 426.33 ± 32.3 | uncompetitive |
| staurosporine | 98.69 ± 7.8 | 69.12 ± 4.6 | competitive | 946.54 ± 71.2 | 455. 39 ± 34.7 | mixed[e] |

[a] ATP-dependent autophosphorylation. [b] Histone phosphorylation. [c] The $IC_{50}$ curves were generated by SigmaPlot regression fitting using the equation: $y = 100. (I_{max}x^n/(IC_{50}^n + x^n))$ ($x$ = [compound], $y$ = % activity, and $I_{max}$ is the maximum percentage of inhibition). [d] $K_i$ was determined from Lineweaver−Burk plot. [e] $K_{is}$ value is shown for mixed inhibition.

Table 2: Comparison of Kinetic Parameters of Wild-Type and Mutant STY Protein Kinase for Tyrosine Kinase Inhibitors

| | ATP[a] | | $K_i$ [c] (nM) | | histone [b] | |
|---|---|---|---|---|---|---|
| protein | tyrphostin | genistein | staurosporine | tyrphostin [d] | genistein | staurosporine [d] |
| WT | 18.31 ± 1.4 | 20.43 ± 1.9 | 69.12 ± 8.7 | 201.55 ± 19.1 | 426.33 ± 39.4 | 455.39 ± 34.7 |
| Y148F | 187.37 ± 15.3 | 191.34 ± 16.5 | 571.01 ± 54.7 | 396.04 ± 45.1 | 819.37 ± 76.2 | 621.32 ± 67.1 |
| Y213F | 14.33 ± 1.1 | 16.97 ± 1.2 | 56.23 ± 6.9 | 251.23 ± 21.2 | 411.89 ± 31.2 | 549.27 ± 72.8 |
| Y297F | 186.14 ± 14.2 | 194.23 ± 1.4 | 464. 21 ± 45.2 | 411.87 ± 79.1 | 855.43 ± 78.2 | 694.22 ± 73.1 |
| Y317F | 54.51 ± 2.9 | 59.41 ± 3.2 | 112.23 ± 10.9 | 355.12 ± 29.2 | 809.23 ± 76.4 | 599.32 ± 43.1 |

[a] ATP-dependent autophosphorylation. [b] Histone phosphorylation. [c] $K_i$ was determined from Lineweaver−Burk plot. [d] $K_{is}$ value is shown for mixed inhibition.

for tyrphostin and genistein toward ATP is increased by 3-fold for Y317F mutant (Table 1). On the other hand, Y213F led to the slight decrease in $K_i$ value for ATP toward all the three inhibitors, suggesting a higher affinity for the inhibitor. The K160R mutant protein of STY protein kinase was inactive. The relative $K_i$ values of the mutants at fixed ATP concentrations are summarized in Table 2.

We have observed linear mixed type noncompetitive inhibition for all the mutant proteins with histone when tyrphostin and staurosporine used. Mutant proteins showed uncompetitive inhibition for genistein with histone (plots not shown). There was no significant difference in the inhibition constants of the tyrosine mutant proteins with respect to wild-type for histone. However, $K_i$ value is increased by 2-fold for Y148F and Y297F mutant proteins for genistein and tyrphostin, and 1.5-fold for staurosporine. There was 1.5−2-fold increase in the $K_i$ of Y317F mutant protein for all the inhibitors. The relative $K_i$ values of the mutations at fixed histone concentrations are summarized in Table 2. These results suggest that $Tyr^{148}$ and $Tyr^{297}$ residues of STY protein kinase play a significant role in the inhibition of autophosphorylation.

## DISCUSSION

Tyrosine phosphorylation plays an important role in growth, development, and oncogenesis in animals (*1*). On the other hand, no tyrosine kinase has hitherto been cloned in plants. Peanut STY protein kinase is shown to be regulated by tyrosine phosphorylation (*3*). To gain insights into the mechanism of tyrosine phosphorylation of recombinant STY protein kinase, we have performed molecular docking and kinetic analysis with tyrosine kinase inhibitors. Here, we report that autophosphorylation of STY protein kinase occurs through an intramolecular mechanism. Furthermore, we were unable to detect in vitro intermolecular phosphorylation of the K160R mutant protein by the recombinant STY protein kinase. In many cases, autophosphorylation of a protein kinase has been shown to proceed by an intermolecular mechanism (*26*) in which the catalytic domains and phosphorylation sites reside on separate molecules. Occurrence of intramolecular autophosphorylation mechanism has been reported for a cytoplasmic tyrosine kinase, Src (*27*). Autophosphorylation of serine/threonine protein kinases in plants has been shown to occur intermolecularly or intramolecularly, but neither of the two mechanisms has been related to a specific form of regulation of activity (*28*−*30*). *Arabidopsis* SOS2, an intracellular serine/threonine protein kinase (*31*) and tomato protein kinases, Pto and Pti1 undergo autophosphorylation via an intramolecular mechanism (*32*).

STY protein kinase has a two-lobe architecture typical of protein kinases. In general, ATP binds in the cleft between the two lobes of protein kinases (*33*, *34*). Crystal structures of the serine/threonine kinases, cyclin-dependent kinase 2 (*35*), casein kinase (CK) 1 (*36*), and PKA (*37*) in complex with various inhibitors have been reported. These structures show that the ATP-binding pocket, although relatively well conserved in the protein kinase family, will accommodate molecules of different chemical structure, which can selectively inhibit protein kinases. Our molecular docking studies revealed that the protein kinase inhibitors bind in the same region as ATP, suggesting a similar mode of regulation for plant protein kinases.

Staurosporine is a potent inhibitor of protein kinases, with an $IC_{50}$ value of 2.7 nM for protein kinase C, 8.2 nM for PKA, 6.4 nM for PTK of p60v-src, and 630 nM for PTK of EGF receptor. Staurosporine was originally thought to be an ATP-competitive inhibitor specific for PKC. More recent studies showed that it is a broad, potent inhibitor of various kinases, including tyrosine kinases, and does not compete with ATP (*38*−*40*). The binding site of staurosporine is likely to overlap with the ATP-binding pocket. Genistein shows inhibitory activity against tyrosine kinases such as the EGF receptor, pp60src, and pp110gag-fes in vitro. Genistein inhibits protein kinases by competing at the ATP-binding site (*41*). Our kinetic analysis revealed that staurosporine and genistein competed with ATP. Tyrphostins are a series of protein tyrosine kinase inhibitors that were originally modeled after the microbial inhibitor erbstatin (*42*). Tyrphostins against EGF inhibited EGF-dependent phosphorylation of exogenous substrates and cellular proliferation (*42*−*44*) as

well as EGF-dependent activation of Src-family kinases (*45*), with $IC_{50}$ values in the micromolar range. STY protein kinase is the first plant kinase shown to be inhibited by tyrphostin.

The inhibitory kinetics with staurosporine and tyrphostin indicated the reduced apparent affinity and maximum velocity of histone for STY protein kinase, suggesting a noncompetitive mixed inhibition pattern. In mixed inhibition kinetics, the binding of substrate or inhibitor induces the conformational change in the enzyme structure interfering with the binding of other molecule. Noncompetitive inhibitors can bind to a form of enzyme that still has substrate bound. In the histone phosphorylation assay, binding of histone to the enzyme might precede binding of staurosporine or tyrphostin. A similar kind of mechanism was seen with protein kinases, namely, PKA, CK1, CK2, MAP kinase (ERK-1), c-Fgr, Lyn, CSK, and TPK-IIB/p38Syk, wherein staurosporine inhibition was competitive with respect to ATP. In contrast, either uncompetitive or noncompetitive kinetics of inhibition with respect to the phosphoacceptor substrate was exhibited by Ser/Thr and Tyr-specific protein kinases (*46*). Kinetic analysis revealed that protein kinase C (PKC) inhibition by Go 6976 was competitive with ATP and noncompetitive with histone (*47*). Levendustin-A (*48*) olomoucine (*49*), sangivamycin (*50*), and quercetin (*51*) competed with ATP and exhibited noncompetitive inhibition with histone. Two-substrate enzyme-catalyzed reactions may proceed by a variety of mechanisms, including the ping-pong bi−bi, compulsory-order ternary complex and random-order ternary complex mechanisms (*24*). It might be possible that staurosporine and tyrphostin bind to the STY protein kinase at multiple places in the reaction pathway and consequently exhibit noncompetitive mixed inhibition kinetics with respect to phosphate acceptor. Differential inhibition of protein kinases is a general phenomenon of staurosporine and related compounds.

Inhibition kinetics of STY protein kinase were uncompetitive with respect to histone, suggesting that the binding of histone at the active site precedes the binding of genistein to the enzyme. Uncompetitive inhibition is rare in one substrate reactions, but common in bisubstrate reactions. Amiloride acts as a competitive inhibitor with ATP and uncompetitive inhibitor with histone (*52*). The kinetics of inhibition of PKC-gamma using staurosporine (*38*) and UCN-01 (*53*) were competitive with ATP and uncompetitive with histone. Under the bisubstrate reaction conditions, genistein might bind to a complex of enzyme, MgATP and histone, and thereby forming a complex that cannot be broken down to products. A detailed understanding of the molecular basis of STY protein kinase inhibition will require crystal structure analysis of the STY kinase−inhibitor complex. Genistein bears no structural relationship to ATP, inhibition of STY protein kinase by genistein may not be due to the true competition for exactly the same site as utilized by ATP. Because of the competitive nature of inhibition with ATP and uncompetitive nature with substrate, the concentrations of these substrates can have dramatically different effects on the degree of inhibition observed.

$K_i$ value is drastically less than the $K_m$ value of ATP for all the inhibitors, suggesting the strong binding. Thus, these inhibitors could be good tools to elucidate the plant cellular processes that are mediated by tyrosine phosphorylation.

Protein kinase inhibitors bind to the ATP-binding site, a highly conserved nucleotide-binding pocket within the kinase domain of protein tyrosine kinases, thereby blocking access of ATP. P-loop and A-loop are the two main targets for binding of the inhibitor to the kinases (*26*). In protein kinases, residues in both the N- and C-terminal lobes bind and thus position ATP for phosphoryl transfer (*34*). The ATP-binding sites in the crystal structures of basal state PTKs also display various degrees of accessibility. The A-loop in the structures of basal state PTKs, including insulin receptor kinase D (*54*), the fibroblast growth factor receptor tyrosine kinase (*14*), Src (*15*), Hck (*55*), and Abl (*17*), exhibit a wide range of conformations. Y148F mutant of ATP-binding loop and Y297F mutant of A-loop resulted in increased $K_i$ value of autophosphorylation toward the inhibitors, suggesting the strong binding of ATP and inhibitors. The response of the kinase proteins could be due to regulatory state of kinase and by tyrosine phosphorylation. We did not observe any significant change in the inhibition constant of the mutant enzymes with respect to wild-type for histone phosphorylation.

In conclusion, this study forms the first report on the inhibition of protein kinases by tyrosine kinase inhibitors in plants. The observation that STY protein kinase is inhibited by tyrosine kinase inhibitors suggests that plant protein kinases are also regulated in a similar manner as mammalian tyrosine kinases. The present study helps in gaining more insights into the mechanism of tyrosine phosphorylation in plants, an otherwise poorly understood area of plant biology.

## REFERENCES


1. Hunter, T. (1995) A thousand and one protein kinases, *Cell 80*, 225−236.
2. Rudrabhatla, P., and Rajasekharan, R. (2002) Developmentally regulated dual-specificity kinase that is induced by abiotic stresses, *Plant Physiol. 130*, 380−390.
3. Rudrabhatla, P., and Rajasekharan, R. (2003) Mutational analysis of stress-responsive peanut dual specificity kinase: Identification of tyrosine residues involved in protein kinase activity, *J. Biol. Chem. 278*, 17328−17335.
4. Bishop, J. M. (1987) The molecular genetics of cancer, *Science 235*, 305.
5. Ullrich, A., and Schlessinger, J. (1990) Signal transduction by receptors with tyrosine kinase activity, *Cell 61*, 203−212.
6. Aaronson, S, A. (1991) Growth factors and cancer, *Science 254*, 1146−1153.
7. Levitzki, A., and Gazit, A. (1995) Tyrosine kinase inhibition: an approach to drug development, *Science 267*, 1782−1788.
8. Groundwater, P. W., Solomons, K. R., Drewe, J. A., and Munawar, M. A. (1996) Protein tyrosine kinase inhibitors, *Prog. Med. Chem. 33*, 233−329.
9. Ruegg, U. T., and Burgess, G. M. (1989) Staurosporine, K-252 and UCN-01: potent but nonspecific inhibitors of protein kinases, *Trends Pharmacol. Sci. 10*, 218−220.
10. Asano, T., Kunieda, N., Omura, Y., Ibe, H., Kawasaki, T., Takano, M., Sato, M., Furuhashi, H., Mujin, T.; Takaiwa. F., et al. (2002) Rice spk, a calmodulin-like domain protein kinase, is required for storage product accumulation during seed development: phosphorylation of sucrose synthase is a possible factor, *Plant Cell 14*, 619−628.
11. Bradford, M. M. (1976) A rapid and sensitive method for quantitation of microgram quantities of protein utilizing the principle of protein-dye binding, *Anal. Biochem. 72*, 248−254.
12. Laemmli, U.K. (1970) Cleavage of structural proteins during the assembly of the head of bacteriophage $T_4$, *Nature 227*, 680−685.
13. Guex, N., and Peitsch, M. C. (1997) SWISS-MODEL and the Swiss-PdbViewer: an environment for comparative protein modeling, *Electrophoresis 18*, 2714−2723.
14. Weijland, A., Williams, J. C., Neubauer, G., Courtneidge, S. A., Wierenga, R. K., and Superti-Furga, G. (1997) Src regulated by

C-terminal phosphorylation is monomeric, *Proc. Natl. Acad. Sci. U.S.A. 94*, 3590−3595.
15. Xu, W., Doshi, A., Lei, M., Eck, M. J., and Harrison, S. C. (1999) Structural basis for selectivity of the isoquinoline sulfonamide family of protein kinase inhibitors, *Mol. Cell 3*, 629−638.
16. Nagar, B., Bornmann, W. G., Pellicena, P., Schindler, T., Veach, D. R., Miller, W. T., Clarkson, B., and Kuriyan, J. (2002) Crystal structures of the kinase domain of c-Abl in complex with the small molecule inhibitors PD173955 and imatinib (STI-571), *Cancer Res. 62*, 4236−4243.
17. Schindler, T., Bornmann, W., Pellicena, P., Miller, W. T., Clarkson, B., and Kuriyan, J. (2000) Structural mechanism for STI-571 inhibition of abelson tyrosine kinase, *Science 289*, 1938−1942.
18. Sippl, M. J. (1993) Recognition of errors in three-dimensional structures of proteins, *Proteins 17*, 355−362.
19. Sayle. R., and Milner-White, E. J. (1995) RasMol: Biomolecular graphics for all, *Trends Biochem. Sci. 20*, 374.
20. Morris, G. M., Goodsell, D. S., Huey, R., and Olson, A. J. (1996) Distributed automated docking of flexible ligands to proteins: parallel applications of AutoDock 2.4, *J. Comput.-Aided Mol. Des. 10*, 293−304.
21. Corbin, J. D. and Reimann, E. M. (1974) Assay of cyclic AMP-dependent protein kinases, *Methods Enzymol. 38*, 287−290.
22. Segel, I. H. (1976) *Enzyme Kinetics*, pp 246−261, Wiley-Interscience, New York.
23. Kuntz, I. D. (1992) Structure-based strategies for drug design and discovery, *Science 257*, 1078−1082.
24. Ring, C. S., Sun, E., McKerrow, J. H., Lee, G. K., Rosenthal, P. J., Kuntz, I. D., and Cohen F. E. (1993) Structure-based inhibitor design by using protein models for the development of antiparasitic agents, *Proc. Natl. Acad. Sci. U.S.A. 90*, 3583−3587.
25. Sanchez, R., and Sali, A. (1998) Large-scale protein structure modeling of the *Saccharomyces cerevisiae* genome, *Proc. Natl. Acad. Sci. U.S.A. 95*, 13597−13602.
26. Johnson, L. N., Noble, M. E., and Owen, D. J. (1996) Active and inactive protein kinases: structural basis for regulation, *Cell 85*, 149−158.
27. Brown, M. T., and Cooper, J. A. (1996) Regulation, substrates and functions of src, *Biochim. Biophys. Acta 1287*, 121−149.
28. Roe, J. L., Durfee, T., Zupan, J. R., Repetti, P. P., McLean, B. G., and Zambryski, P. C. (1997) TOUSLED is a nuclear serine/threonine protein kinase that requires a coiled-coil region for oligomerization and catalytic activity, *J. Biol. Chem. 272*, 5838−5845.
29. Horn, M. A., and Walker, J. C. (1994) Biochemical properties of the autophosphorylaton of RLK5, a receptor-like protein kinase from *Arabidopsis thaliana*, *Biochim. Biophys. Acta 1208*, 65−74.
30. Chulze-Muth, P., Irmler, S., Schrder, G., and Schrder, J. (1996) Novel type of receptor-like protein kinase from a higher plant (*Catharanthus roseus*). cDNA, gene, intramolecular autophosphorylation, and identification of a threonine important for auto- and substrate phosphorylation, *J. Biol. Chem. 271*, 26684−26689.
31. Gong, D., Guo, Y., Jagendorf, A. T., and Zhu, J. K. (2002) Biochemical characterization of the *Arabidopsis* protein kinase sos2 that functions in salt tolerance, *Plant Physiol. 130*, 256−264.
32. Sessa, G., D'Ascenzo, M., Loh, Y.-T., and Martin, G. B. (1998) Biochemical properties of two protein kinases involved in disease resistance signaling in tomato, *J. Biol. Chem. 273*, 15860−15865.
33. Mohammadi, M., Schlessinger, J., and Hubbard, S. R. (1996) Structure of the FGF receptor tyrosine kinase domain reveals a novel autoinhibitory mechanism, *Cell 86*, 577−587.
34. Taylor, S. S., and Radzio-Andzelm, E. (1994) Three protein kinase structures define a common motif, *Structure 2*, 345−355.
35. DeAzevedo W. F. J., Mueller-Dieckmann H. J., Schulze-Gahmen U., Worland P. J., Sausville E., and Kim S. H. (1996) Structural basis for specificity and potency of a flavonoid inhibitor of human CDK2, a cell cycle kinase, *Proc. Natl. Acad. Sci. U.S.A. 93*, 2735−2740.
36. Xu, R.-M., Carmel, G., Kuret, J., and Cheng, X. (1996) Crystal structures of c-Src reveal features of its autoinhibitory mechanism, *Proc. Natl. Acad. Sci. U.S.A. 93*, 6308−6313.
37. Engh, R. A., Girod, A., Kinzel, V., Huber, R., and Bossemeyer, D. (1996) Crystal structures of catalytic subunit of camp-dependent protein kinase in complex with isoquinolinesulfonyl protein kinase inhibitors h7, h8, and h89. Structural implications for selectivity, *J. Biol. Chem. 271*, 26157−26164.
38. Ward, N. E., and O' Brian, C. A. (1992) Kinetic analysis of protein kinase C inhibition by staurosporine: evidence that inhibition entails inhibitor binding at a conserved region of the catalytic domain but not competition with substrates, *Mol. Pharmacol. 41*, 387−392.
39. Tamaoki, T., Nomoto, H., Takahashi, I., Kato, Y., Morimoto, M., and Tomita, F. (1986) Staurosporine, a potent inhibitor of phospholipid/Ca++dependent protein kinase, *Biochem. Biophys. Res. Commun. 135*, 397−402.
40. Ruegg, U. T., and Burgess, G. M. (1989) Staurosporine, K-252 and UCN-01: potent but nonspecific inhibitors of protein kinases, *Trends Pharmacol. Sci. 10*, 218−220.
41. Akiyama, T., Ishida, J., Nakagawa, S., Ogawara, H., Watanabe, S., Itoh, N., Shibuya, M., and Fukami, Y. (1987) Genistein, a specific inhibitor of tyrosine-specific protein kinases, *J. Biol. Chem. 262*, 5592−5595.
42. Yaish, P., Gazit, A., Gilon, C., and Levitzki, A. (1988) Blocking of EGF-dependent cell proliferation by EGF receptor kinase inhibitors, *Science 242*, 933−935.
43. Osherov, N., Gazit, A., Gilon, C., and Levitzki, A. (1993) Selective inhibition of the epidermal growth factor and HER2/neu receptors by tyrphostins, *J. Biol. Chem. 268*, 11134−11142.
44. Gazit, A., Chen, J., App, H., MacMahon, G., Hirth, P., Chen, I., and Levitzki, A. (1996) Tyrphostins IV- -highly potent inhibitors of EGF receptor kinase. Structure−activity relationship study of 4-anilidoquinazolines, *Bio. Org. Med. Chem. 4*, 1203−1207.
45. Osherov, N., and Levitzki, A. (1994) Epidermal-growth-factor-dependent activation of the src-family kinases, *Eur. J. Biochem. 225*, 1047−1053.
46. Meggio, F., Donella Deana, A., Ruzzene, M., Brunati, A. M., Cesaro, L., Guerra, B., Meyer, T., Mett, H., Fabbro, D., and Furet, P, et al. (1995) Different susceptibility of protein kinases to staurosporine inhibition. Kinetic studies and molecular bases for the resistance of protein kinase CK2, *Eur. J. Biochem. 234*, 317−322.
47. Martiny-Baron, G., Kazanietz, M. G., Mischak, H., Blumberg, P. M., Kochs, G., Hug, H., Marme, D., and Schachtele, C. (1993) Selective inhibition of protein kinase C isozymes by the indolocarbazole Go 6976, *J. Biol. Chem. 268*, 9194 - 9197.
48. Onoda, T., Iinuma, H., Sasaki, Y., Hamada, M., Isshibi, K., Naganawa, H., Takeuchi, T., Tatsuta, K., and Umezawa, K. (1989) Isolation of a novel tyrosine kinase inhibitor, lavendustin A, from *Streptomyces griseolavendus*, *J. Nat. Prod. (Lloydia) 52*, 1252−1257.
49. Vesely, J., Havlicek, L., Strnad, M., Blow, J. J., Donella-Deana, A., Pinna, L., Letham, D. S., Kato, J., Detivaud, L., Leclerc, S, et al. (1994) Inhibition of cyclin-dependent kinases by purine analogues, *Eur. J. Biochem. 224*, 771−786.
50. Loomis, C. R., and Bell, R. M. (1988) Sangivamycin, a nucleoside analogue, is a potent inhibitor of protein kinase C, *J. Biol. Chem. 263*, *1682*-1692.
51. Graziani, Y., Erikson, E., and Erikson, R. L. (1983) The effect of quercetin on the phosphorylation activity of the Rous sarcoma virus transforming gene product *in vitro* and *in vivo*, *Eur. J. Biochem. 135*, 583−589.
52. Davis, R. J., and Czech, M. P. (1985) Amiloride directly inhibits growth factor receptor tyrosine kinase activity, *J. Biol. Chem. 260*, 2543−2551.
53. Seynaeve, C. M., Kazanietz, M. G., Blumberg, P. M., Sausville, E. A., and Worland, P. J. (1994) Differential inhibition of protein kinase C isozymes by UCN-01, a staurosporine analogue, *Mol. Pharmacol. 145*, 1207−1214.
54. Hubbard, S. R., Wei, L., Ellis, L., and Hendrickson, W. A. (1994) Crystal structure of the tyrosine kinase domain of the human insulin receptor, *Nature 372*, 746−754.
55. Schindler, T., Sicheri, F., Pico, A., Gazit, A., Levitzki, A., and Kuriyan, J. (1999) Crystal structure of Hck in complex with a Src family selective tyrosine kinase inhibitor, *Mol. Cell 3*, 639−648.

BI0497042